

**THE STARBURST-AGN CONNECTION:
A Spitzer Search for AGN in IR-Selected Starburst Galaxies**

T. G. DIXON¹ & R. D. JOSEPH²

July 24, 2011

Received _____; accepted _____

ABSTRACT

We present observations of a sample of 28 LIRGs from the IRAS Bright Galaxy Catalog. These galaxies were previously observed by Goldader et al. (1997) using $2\mu\text{m}$ spectroscopy on UKIRT. They found that stellar population synthesis models constrained by the spectroscopic diagnostics implied star formation rates that accounted for their infrared luminosities, and there was also no spectroscopic evidence for "buried" AGN at $2\mu\text{m}$. To search for evidence of AGN buried deeply in extinction we have supplemented the UKIRT spectra with Spitzer mid-infrared (5.2 to $38.0\mu\text{m}$) spectra. Using a variety of spectroscopic diagnostics we find that $\sim 50\%$ of the sample shows some evidence for an AGN. We also find that the luminosity of about $\sim (17 \pm 4)\%$ of our sample is probably dominated by emission from AGN, and the remaining $\sim (80 \pm 4)\%$ have luminosities dominated by starbursts. Since $\sim 50\%$ of the sample shows some evidence of concurrent AGN and starburst activity this suggests that both AGN and starbursts commonly coexist in the LIRGS phase of evolution. The sample consists of galaxies that show no AGN signatures at wavelengths less than $2\mu\text{m}$, so it appears that at wavelengths below $2\mu\text{m}$ extinction in these galaxies masks the detection of AGN in these and other LIRGs.

Subject headings: galaxies: starburst - galaxies: active - galaxies: evolution - galaxies: infrared

¹Institute for Astronomy, University of Hawaii, 2680 Woodlawn Drive, Honolulu, HI 96822; dixon@ifa.hawaii.edu.

²Institute for Astronomy, University of Hawaii, 2680 Woodlawn Drive, Honolulu, HI 96822; joseph@ifa.hawaii.edu.

1. Introduction

Since the discovery of a large population of luminous infrared galaxies (LIRGs, $10^{11}L_{sun} \geq L_{(8-1000)\mu m} < 10^{12}L_{sun}$) (e.g. Rieke & Low (1972)) there has been controversy concerning the energy sources that power these galaxies. Both AGN and recent bursts of star formation ("starbursts") were proposed as the underlying energy sources powering these galaxies, and this has become known as the "Starbursts-Monsters" Controversy (Heckman et al. 1983). This controversy has reached its apotheosis in attempts to understand the more luminous ULIRGs ($L_{(8-1000)\mu m} \geq 10^{12}L_{sun}$), but that is not the subject of this paper. Both AGN and starbursts are widely acknowledged to exist deeply buried in interstellar dust, and the extinction problem has made it difficult to reach an incontrovertible conclusion. In particular, those who have favored AGN but failed to find the diagnostics indicative of AGN activity have argued that there must be too much extinction to see evidence of an AGN at optical or near-infrared wavelengths (e.g. Sanders (1999)), whereas those favoring starbursts have argued that, in the majority of cases all the diagnostic evidence available indicates that recent star formation accounts for the bolometric luminosity (e.g. Joseph (1999)).

Most LIRGs are recognized to have morphological features, such as tidal bridges and tails, characteristic of interacting or merging galaxies (Toomre & Toomre 1972). Joseph et al. (1984); Joseph & Wright (1985); Wright et al. (1988) and others, have shown that interactions and mergers of spiral galaxies are effective triggers of starbursts. In fact, Larson & Tinsley (1978) compared the UVB colors of galaxies in Arp's peculiar galaxy catalog to those of a control sample, and showed that the greater dispersion in the colors of the interacting galaxies could be understood as the result of recent star formation triggered by interactions.

Evidence has been accumulating that starburst activity is sometimes present in the

central regions of Seyfert 2 galaxies. A number of optical studies have revealed evidence for starburst activity in a (generally minor) fraction of Seyfert 2 galaxies (Rodriguez Espinosa et al. 1987; Shier et al. 1996; Heckman et al. 1983; Cid Fernandes et al. 2001; Storchi-Bergmann et al. 2001). In fact, the prototypical Seyfert 2 galaxy NGC 1068 is an excellent example. Sani et al. (2010) have found evidence for intense on-going star formation in a sample of narrow-line Seyfert 1 galaxies. These results suggest that there may be a connection between starburst and AGN activity.

This idea has gained strong support from modeling of interactions and mergers. Numerical simulations of gas-rich spiral galaxy mergers that have included gas dynamics have supported the notion that major mergers between gas-rich spirals do lead to rapid star formation (Noguchi 1988; Barnes & Hernquist 1991, 1992; Schweizer 2005). Mihos & Hernquist (1996) and Hopkins et al. (2010) have done high-resolution hydrodynamic simulations for the formation of starbursts and AGN in mergers, and then modelled the relative contributions of "normal" galaxy discs, merger-induced starbursts, and merger-induced AGN to predict the contributions of all three to the total infrared luminosities of galaxies as they evolve from high to low redshift. Their results indicate that, while merger-induced star formation dominates the merger-induced AGN contribution to the infrared luminosity, both processes should be present in mergers for at least a fraction of the merger evolution timescale.

Goldader et al. (1997) identified a subset of a complete sample of LIRGs selected from the IRAS Bright Galaxy Catalog (Soifer et al. 1987), which is a statistically complete sample of 324 galaxies visible from the northern hemisphere at galactic latitudes of 30 or larger. Goldader limited their sample to 97 systems (several objects were clearly interacting) with $L_{IR} \geq 10^{11.2} L_{sun}$, declination between -40° and $+60^\circ$ that could be observed with UKIRT telescope. Of these 97 systems, Goldader et al. (1997) observed 43 systems using K-band

spectroscopy on the UKIRT. Goldader et al. (1997) showed that starburst models were consistent with the K-band fluxes and that star formation accounted for the total infrared luminosities of the sample. Moreover there was no evidence of AGN activity in the K-band that had not previously been observed in the optical spectra of these galaxies. However, the question has remained whether extinction was still a significant factor even at $2\mu\text{m}$. We have therefore used the Spitzer IRS mid-infrared spectrometer to obtain mid-infrared diagnostics for 28 LIRGs from the Goldader et al. (1997) sample. These 28 LIRGs showed no AGN signatures in optical or near infrared. The primary aim was to search for AGN features in the mid-infrared ($5 - 35\mu\text{m}$), which would be even less subject to extinction than $2\mu\text{m}$ spectra, in order to investigate the putative connection between starbursts and AGN in powering LIRGs. We also hoped to be able to estimate the contribution of AGN to the L_{FIR} of the sample. We note that our sample of 28 galaxies will include only AGN that are too deeply buried in extinction to be detected in either the optical or the K-band. Thus there may be differences between the results for our sample and samples that include optically classified AGN. Throughout this paper we adopt the cosmology $H_0 = 75 \text{ km s}^{-1} \text{ Mpc}^{-1}$ and $q_0 = 0$

After this manuscript was submitted we learned that Petric et al. (2011) had a similar study of LIRGs in press. In the Discussion Section we compare our results with those found by Petric et al.

2. OBSERVATIONS

This paper is based on Spitzer (Werner et al. 2004) IRS observations of 28 LIRG galaxies from the IRAS Bright Galaxy Samples of Soifer et al. (1987), listed in Table 1. The Spitzer Infrared Spectrograph, IRS (Houck et al. 2004), provides unprecedented mid-infrared sensitivity for low and moderate resolution spectroscopy from 5.2 to $38.0\mu\text{m}$.

IRS is composed of four separate modules, with two modules providing a spectral resolution $R \sim 60$ -120 over 5.2-38.0 μm and two modules providing a spectral resolution $R \sim 600$ over 9.9-37.2 μm . For the work herein we used three of the four Spitzer modules; the long wavelength low resolution module (LL) was not used. For target acquisition the "no peak-up" option was used. The data were processed through the Spitzer Science Center's IRS pipeline data reduction software. This performs standard data reduction tasks such as dark current subtraction. We used the IRSClean application to correct for hot or bad pixels.

3. DIAGNOSTIC TOOLS

Mid-infrared spectroscopy provides a variety of diagnostics of both starburst and AGN activity, as previously done by (Veilleux et al. 2009; Genzel et al. 1998; Sturm et al. 2002) and others. The ion $[\text{NeV}]$ has an ionization potential of 97 eV and so the coronal lines at 14.3 μm and 24.3 μm are good indicators of the presence of an AGN (Spinoglio & Malkan 1992). Conversely, the $[\text{NeII}]12.8\mu\text{m}$ line is strong in the HII regions of starburst galaxies but is generally weak in AGN. Thus the line ratios $[\text{NeV}]14.3\mu\text{m} / [\text{NeII}]12.8\mu\text{m}$ and $[\text{NeV}]24.3\mu\text{m} / [\text{NeII}]12.8\mu\text{m}$ can be used to identify galaxies that contain AGN (Genzel et al. 1998). Sturm et al. (2002), have measured the above lines using ISO-SWS for a sample of 29 AGN galaxies. For their AGN sample the $[\text{NeV}]14.3\mu\text{m} / [\text{NeII}]12.8\mu\text{m}$ and $[\text{NeV}]24.3\mu\text{m} / [\text{NeII}]12.8\mu\text{m}$ line ratios have a median values of 0.45 and 0.35 respectively. The same line ratios in starburst galaxy that do not contain any AGN have values that are one or two orders lower in magnitude (Genzel et al. 1998).

A strong $[\text{OIV}]25.9\mu\text{m}$ line is often detected in LIRGs. The $[\text{O IV}]$ ion has a lower ionization potential of 55 eV and can be weakly produced in starburst galaxies by supernovae and strong wind shocks. Nevertheless, while strong $[\text{O IV}]$ lines are found

in AGN they are never strong when observed in starburst galaxies (Sturm et al. 2002), making a strong $[OIV]25.9\mu m / [NeII]12.8\mu m$ ratio a good diagnostic for the presence of an AGN. For the Sturm et al. (2002) sample of AGN, the $[OIV]25.9\mu m / [NeII]12.8\mu m$ ratio has a median value of about 1. In the galaxy templates used by Genzel et al. (1998), the $[OIV]25.9\mu m / [NeII]12.8\mu m$ is typically one to two orders of magnitude lower in starburst galaxies than in AGN galaxies.

The $[NeIII]15.6\mu m / [NeII]12.8\mu m$ ratio can be used to determine the temperature of an emitting region. In the case of starburst galaxies this ratio is typically 0.1 or lower (Ho & Keto 2007), while in galaxies that host an AGN this ratio is expected to be about 1 or larger. The AGN galaxies of Sturm et al. (2002), have a median $[NeIII]15.6\mu m / [NeII]12.8\mu m$ of 1.1 and we use this value to indicate the presence of an AGN in our sample.

PAH (Polycyclic Aromatic Hydrocarbon) emission features are extremely strong in starburst galaxies but are weak or absent in AGN (Roche et al. 1991; Tielens et al. 2004). We use the strength of the $PAH\ 7.7\mu m$ feature as described by Lutz et al. (1998) to indicate the presence or absence of an AGN. The $PAH\ 7.7\mu m$ strength is determined by measuring the peak at $7.7\mu m$ and subtracting the continuum value at $7.7\mu m$. The continuum at $7.7\mu m$ is determined by linearly interpolating between the continuum point at $5.9\mu m$ and the continuum point at $10.9\mu m$. Lutz et al. (1998), suggest that a $PAH\ 7.7\mu m$ strength < 1 is a good indicator of an AGN. In the starburst templates of Genzel et al. (1998), the median $PAH\ 7.7\mu m$ strength is 3.1, while the median $PAH\ 7.7\mu m$ for their AGN templates is 2.4. As well as using the $PAH\ 7.7\mu m$ feature as a diagnostic in its own right, we also use the $[OIV]25.9\mu m / [NeII]12.8\mu m$ versus the $PAH\ 7.7\mu m$ strength with the Genzel et al. (1998) calibration curve to measure the contribution of AGN to each galaxy’s L_{FIR} .

AGN produce a warm dust component in the mid-infrared and the strength of continuum flux ratios such as the $IRAS_{5.9\mu m}$ to $IRAS_{60\mu m}$, $IRAS_{25\mu m}$ to $IRAS_{60\mu m}$ and

$f_{30\mu m}$ to $f_{15\mu m}$ (Lutz et al. 1998; Farrah et al. 2007; Veilleux et al. 2009) have been found to correlate with the presence of AGN. We use the continuum ratio $\log\left(\frac{f_{30}}{f_{15}}\right)$ to measure the strength of the warm dust component in each galaxy. Veilleux et al. (2009) find that starburst galaxies have $\log\left(\frac{f_{30}}{f_{15}}\right) = 1.55$ while AGN have $\log\left(\frac{f_{30}}{f_{15}}\right) = 0.2$.

In the mid-infrared, the spectral energy distribution of an AGN is well fit by a power-law. Conversely, the mid-infrared spectra of starburst galaxies have strong *PAH* $7.7\mu m$ emission and strong $10\mu m$ silicon absorption features that readily distinguish these from a simple power-law spectral shape. One caveat however is that the power-law fit is most appropriate for QSOs or Seyfert 1 AGN. Seyfert 2 AGN still have moderate *PAH* $7.7\mu m$ emission and $10\mu m$ silicon absorption features, though these are weaker than in starburst galaxies (Veilleux et al. 2009). We use the $7\text{-}14\mu m$ portion of our low resolution spectra and fit a line to the $\log(f_\nu)$ versus $\log(\lambda)$ to determine the spectral index and goodness of fit for a power-law for each galaxy.

In summary we use seven basic diagnostics. We use four MIR line ratios, i) $[NeIII]15.6\mu m / [NeII]12.8\mu m$, ii) $[NeV]14.3\mu m / [NeII]12.8\mu m$, iii) $[NeV]24.3\mu m / [NeII]12.8\mu m$, and iv) $[OIV]25.9\mu m / [NeII]12.8\mu m$. We use two continuum diagnostics i) a fit to the MIR spectral-slope and ii) the $\log\left(\frac{f_{30}}{f_{15}}\right)$ ratio. We also use the strength of the *PAH* $7.7\mu m$ feature. An eighth diagnostic that is somewhat more sophisticated is produced by combining the *PAH* $7.7\mu m$ strength with the $[OIV]25.9\mu m / [NeII]12.8\mu m$ ratio. Using the calibration curve of Genzel et al. (1998) this eighth diagnostic can be used to estimate the contribution of an AGN to each galaxy's luminosity.

4. DATA ANALYSIS

4.1. Line Ratios and PAH features

Table 2 shows the observed values of the line ratios $[NeV]14.3\mu m / [NeII]12.8\mu m$, $[NeV]24.3\mu m / [NeII]12.8\mu m$ and $[OIV]25.9\mu m / [NeII]12.8\mu m$. These ratios are also shown in Fig. 1 and are derived from the spectral line fluxes in Table 3. We have linearly interpolated between the AGN and starburst values of these line ratios to get an estimated of the AGN contribution to each galaxy's L_{FIR} . Five Galaxies (18% of the sample) have $[NeV]14.3\mu m / [NeII]12.8\mu m$, $[NeV]24.3\mu m / [NeII]12.8\mu m$ or $[OIV]25.9\mu m / [NeII]12.8\mu m$ values that are more than 50% of the median value found in AGN by Sturm et al. (2002). Thus the power output of these may be dominated by the power output of their AGN. Additionally, three galaxies (11% of the sample) have line ratios of more than 25% of the median value seen in AGN, suggesting that these galaxies may also have some AGN contribution to their power output.

The $[NeII]12.8\mu m$ line is detected in all galaxies except Arp302 and the $[NeIII]15.6\mu m$ line is detected in all galaxies except galaxies MCG+08-18-012, IR10173-0828 and Arp302. Table 4 shows the measured $[NeIII]15.6\mu m / [NeII]12.8\mu m$ values. Two galaxies (Zw 448.020, MCG+07-23-019, 7% of the sample) have $[NeIII]15.6\mu m / [NeII]12.8\mu m$ ratios > 1 , which indicates that these galaxies have strong contributions to their luminosity from AGN.

The $PAH7.7\mu m$ strengths given in Table 3 and plotted in Fig. 2 show that 6 galaxies (21%) have PAH strengths of < 1 which suggests that AGN make a significant contribution to the lumionsity of these galaxies. Additionally, 5 galaxies (18%) have $PAH7.7\mu m$ strengths < 2.1 (which is the average PAH strength found in the AGN sample of Genzel et al. (1998)), consequently, these galaxies may also have AGN contributing to

their luminosity.

Fig. 3 shows the measured $[OIV]25.9\mu m / [NeII]12.8\mu m$ line ratios, the $PAH\ 7.7\mu m$ strengths and the calibration curve of Genzel et al. (1998). This curve has been used to estimate quantitatively the contribution of an AGN to each galaxy's power output. Three galaxies (11%) in our sample have the low $PAH\ 7.7\mu m$ strengths and high $[OIV]25.9\mu m / [NeII]12.8\mu m$ ratios characteristic of galaxies dominated by AGN. An additional 12 galaxies (43%) of our sample have locations on the Genzel curve that suggest they have from 5-50% of their luminosity provided by an AGN. Using the Genzel curve the total L_{FIR} contribution of AGN to the L_{FIR} of our sample is $(17 \pm 4) \%$.

4.2. Mid-Infrared Spectral Energy Distributions

In the 7-14 μm range, 6 galaxies (21%) have mid-infrared spectra that are well fit by a power-law of the form $F_\nu \propto \lambda^{-\alpha}$. This power-law shape is characteristic of AGN spectral energy distributions, and suggests that AGN may be dominating the output of these galaxies. The remaining 22 galaxies in the sample are not well fit by a power-law and show strong $PAH\ 7.7\mu m$ and strong 10 μm silicon absorption features, suggesting that these galaxies are dominated by energy produced in starburst regions. The power-law spectral indices and uncertainties for these six galaxies are shown in Table 5 while Fig. 4 shows the best fit spectral indices for the all of the LIRG sample. Those that have obvious power-law shapes rather than starburst like shapes (i.e. with strong broad $PAH\ 7.7\mu m$ emission and 10 μm silicon absorption features) have significantly larger spectral indices (typically $\alpha > 3$). Fig. 5 shows in the upper panel, the six AGN-like spectra (normalized to have an area of 1.0 under the curve). The middle panel in this figure shows a similar plot for the normalized spectra of the starburst-like galaxies in our sample. In the same figure the bottom panel shows a plot of the average of the six AGN-like normalized spectra and the average of the

starburst like spectra. The averaged spectra in Fig.5 have very different spectral slope and a different structure in the mid-infrared.

The starburst-averaged spectrum has a strong *PAH* $7.7\mu m$ feature and a strong $10\mu m$ silicon absorption features, while in the AGN averaged spectrum these features are weak or absent and the spectrum has a power-law shape. PAH features are usually observed to be prominent in starburst galaxies, and a good correlation between the strength of PAH features and IR luminosity has been demonstrated for starburst galaxies by Brandl et al. (2006). However, PAH features are generally weak or absent in AGN (Weedman et al. 2005), but the nature of PAH features and their use as indicators of star formation is still poorly understood (Peeters et al. 2004). The absence of PAH features in AGN is thought to be due to a combination of two factors. First, AGN have a harder radiation field than is found in starburst galaxies. This is generated by the AGN's accretion disk and is thought to destroy the PAHs. Second, in a luminous AGN the mid-infrared continuum is extremely strong and can wash-out the PAH features even if there is a high rate of star formation (Laurent et al. 2000). This power-law spectral shape in the mid-infrared is a fast and efficient way of selecting galaxies that are candidates for AGN-dominated galaxies. We note that all but one of the galaxies (Arp302) that have an AGN power-law like spectral shape also have $[NeV]24.3\mu m / [NeII]12.8\mu m$, $[NeV]14.3\mu m / [NeII]12.8\mu m$, or $[OIV]25.9\mu m / [NeII]12.8\mu m$ values and *PAH* $7.7\mu m$ strengths that suggest a significant AGN contribution to their luminosity. In the case of Arp302 we detect no high ionization lines. However, Arp302 does have a weak PAH strength and weak [Ne II] and [S III] lines which are also characteristics of AGN.

4.3. $\log\left(\frac{f_{30\mu m}}{f_{15\mu m}}\right)$ Continuum Ratio

To distinguish between AGN and starburst galaxies we use the values determined by Veilleux et al. (2009) for the $\log\left(\frac{f_{30}}{f_{15}}\right)$ continuum ratio and following Veilleux et al. (2009), we interpolate between these values to give an estimate of the percentage L_{FIR} contribution from the AGN component of each galaxy (Table 3 shows the estimated AGN percentage contribution based on the $\log\left(\frac{f_{30}}{f_{15}}\right)$). Six galaxies (21% of our sample) have $\log\left(\frac{f_{30}}{f_{15}}\right)$ values suggesting that an AGN contributes $> 50\%$ to their energy output.

4.4. Comparison with Existing Galaxy Classifications and Surveys

To test the assumption that AGN have not previously been observed in the optical or near infrared for our sample of galaxies, we searched NASA’s Extragalactic Database (NED) and references therein for optical and infrared galaxy classifications of our sample. Of the 28 galaxies in our sample, 22 galaxies have classifications in NED (the NED classifications are summarized in Table 6). One galaxy (MCG +00-29-023), has been previously classified as a Seyfert2-LINER combination. The remaining 21 galaxies are classified in NED as a combination of LINERs, LIRGS and starburst galaxies with no evidence of AGN activity in the optical or infrared.

5. Extinction

We have assumed that no significant extinction correction is needed for data at these relatively long wavelengths. We justify this assumption by using the ratio $[SIII]18.7\mu m / [SIII]33.5\mu m$ (shown in Fig. 6 and in Table 4) to estimate a lower limit for extinction (Genzel et al. 1998; Verma et al. 2003). The $[SIII]33.5\mu m$ line was detected in all galaxies and the $[SIII]18.7\mu m$ line was detected in all but two galaxies (MCG+08-18-012,

IR010173-0828) and so we have no extinction estimate for these two galaxies. The [S III] ratio is expected to have a value of ~ 0.5 and be insensitive to the shape of the radiation field and independent of the ionization parameter for $n_e < 10^{2.5} \text{cm}^{-3}$. This ratio does increase with electron density and hence can provide only a lower limit to the relative extinction between these lines. Using the extinction curve of Draine (1989), and assuming the extinction at $33.5\mu\text{m}$ is negligible, we have also estimated a lower limit for A_v (see Table 4). Fig. 6 shows a plot of 0.5 times $[SIII]33.5\mu\text{m}$ versus $[SIII]18.7\mu\text{m}$. The dashed line on this figure is the line of zero relative extinction between the two [S III] lines. Galaxies suffering high extinction will fall below this line. For all other galaxies the relative extinctions calculated from the [S III] ratio are small and the spread of data points around the zero extinction line is primarily due to the uncertainty in the line flux measurements.

6. Discussion

The present sample of 28 LIRGs was selected from a larger sample of 47 LIRGs (43 systems) observed by Goldader et al. (1997). This sample of 28 LIRGs included only LIRGs that showed no indications of AGN in the optical or near infrared. This looked to be strong evidence that there were no AGN buried in dust, since the extinction at $2.2\mu\text{m}$ is about ten times less than that in the visible. Moreover, the $2.2\mu\text{m}$ spectroscopic diagnostics indicate that the infrared luminosities could be completely understood in terms of a recent burst of star formation.

How does this conclusion change in view of the Spitzer mid-infrared spectroscopy reported here? First, we can confirm that these galaxies *all* have significant on-going star formation. The estimated star formation rate for each galaxy can be found in Table 3. These estimates were produced using the calibration of Ho & Keto (2007) to convert $(L_{[NeII]} + L_{[NeIII]})$ to a star formation rate. The average star formation rate is about 50

solar masses per year, and the total star formation rate accounts for $\sim (80 \pm 4)\%$ of the L_{FIR} of the LIRG sample.

Second, and perhaps more surprisingly, one or more mid-infrared lines which are almost certainly due to AGN, $[NeV]14.3\mu m$, $[NeV]24.3\mu m$, or strong $[OIV]25.9\mu m$, are detected in nearly half the sample, as may be seen in Table 3. Consequently, there is conclusive evidence for the co-existence of AGN and starbursts in half of this sample, *none of which showed any evidence for AGN in optical or near-infrared spectroscopy*. And so a second conclusion from this study is that LIRGs—even those selected as having no evidence for AGN at wavelengths as long as $2\mu m$ —frequently exhibit the presence of both AGN and starbursts, if one observes them at longer infrared wavelengths less affected by extinction. This provides further evidence complementing the studies referred to in the Introduction that find starbursts associated with AGN. In this case it is AGN that are found in a sample of classic LIRGs that had been previously classified as starbursts. And while a correlation does not prove there is a causal connection, these results do suggest that processes which stimulate starbursts also may result in triggering the onset of AGN, as suggested in the modeling of Hopkins et al. (2010) and others.

Third, what does one learn about the relative dominance of starbursts or AGN in producing the large infrared luminosities of these galaxies? Seven galaxies (25% of the sample) have significant AGN signatures for at least three of the seven basic diagnostics used to detect AGN. (Table 7 shows a summary of the results of applying each diagnostic. The median percentage of AGN detections by all seven diagnostics is 18%. In addition, using the Genzel et al. (1998) diagnostic curve to estimate the contribution of AGN we find 3 galaxies (11% of the sample, IR01364-1042, MCG+08-18-012, IR10173-0828) in which AGN contribute more than 50% of the L_{FIR} . Consequently the luminosities of these 3 galaxies are probably dominated by the output of their AGN. Also using the Genzel et al. (1998)

curve, we find that a further 12 galaxies, 43% of the sample, mcg-03-04-014, NGC695, ugc3094, NGC2342, NGC2388, NGC3110, ARP193, IZw107N, IR16164-0746, NGC 6286, ESO 602-G025, ZW 453.062, have AGN that contribute between 5-50% of the galaxy’s luminosity. Counting the total contribution of AGN given by the Genzel et al. (1998) curve we find that $\sim (17 \pm 4)\%$ of the total L_{FIR} of the sample is produced by AGN. Additionally, using linear interpolation, the basic diagnostics suggest the following estimated AGN contribution to the total L_{FIR} of the sample, $\frac{[NeV]14.3\mu m}{[NeII]12.8\mu m} = 16\%$, $\frac{[NeV]24.3\mu m}{[NeII]12.8\mu m} = 15\%$, $\frac{[OIV]25.9\mu m}{[NeII]12.8\mu m} = 11\%$, $\frac{[NeIII]15.6\mu m}{[NeII]12.8\mu m} = 18\%$, $\log\left(\frac{f_{30}}{f_{15}}\right) = 44\%$ and $PAH\ 7.7\mu m = 38\%$. These give a median value for the AGN contribution from the basic diagnostics of 17%. The wide variation in the contribution estimates for the simple diagnostics is in part due to the roughness of linearly interpolating between AGN and starburst values and in part due to the fact that real AGN and starbursts have values that are scattered around the assumed AGN and starburst values that were used as the end points for each interpolation.

Previous studies of ULIRGs (Genzel et al. 1998; Lutz et al. 1998; Armus et al. 2007; Farrah et al. 2007) have found 20-30% of ULIRGs have luminosities dominated by an AGN. More recent multiwavelength observations of both LIRGs and ULIRGs by Kartaltepe et al. (2010) found that about 10% of LIRGS and about 40% of ULIRGS were likely to be dominated by the luminosity of an AGN. While these are somewhat rough numbers, they do suggest that a slightly higher fraction of ULIRGs may be dominated by an AGN compared to those of LIRGs.

A recent paper by Petric et al. (2011), provides a statistical analysis of the Spitzer spectra for 248 LIRGS. Spectra for individual galaxies is not given, but since the data has been taken from the Spitzer archive, it will include the data for the 28 LIRGs presented herein. Petric et al. (2011) find a median AGN contribution of 12% to the luminosity of local LIRGS, which is consistent with the 17% found for our LIRG sample.

7. Summary and Conclusions

Mid-infrared spectroscopy has been obtained for a sample of 28 LIRGs, none of which showed evidence of AGN in the optical or in $2.2\mu m$ infrared spectroscopy. Seven basic diagnostics were applied to search for AGN in these galaxies (the results of which are summarized in Table 7). Two of these diagnostics (the $[OIV]25.9\mu m / [NeII]12.8\mu m$ and the $PAH\ 7.7\mu m$ strength) were used with the Genzel et al. (1998) calibration curve to estimate the contribution of AGN to each galaxy’s far infrared luminosity. Additionally the $(L_{[NeII]} + L_{[NeIII]})$ was used to estimate the star formation rate of each galaxy. Our results lead to the following conclusions.

1. There is active star formation present in the entire sample.
2. The average estimated star formation rate per galaxy is 50 solar masses per year and the total star formation accounts for about $(80 \pm 4)\%$ of the total FIR luminosity.
3. The median fraction of AGN detections for all seven simple diagnostics is 18% and there are 11 galaxies (39% of the sample) in which at least two of the seven simple diagnostics suggest the presence of an AGN. These diagnostics indicate that there may be AGN in $\sim 57\%$ of our LIRG sample. Using the Genzel et al. (1998) diagnostic, we found 3 galaxies (11% of the sample) that may be dominated by AGN and a further 12 galaxies (43% of the sample) that have between 5-50% of their luminosity provided by AGN. The Genzel et al. (1998) diagnostic curve thus indicates that $\sim 54\%$ of our LIRG sample may have AGN.
4. Using the diagnostic curve of Genzel et al. (1998) we estimated that AGN contribute $\sim (17 \pm 4)\%$ of the total L_{FIR} of the sample. Using the basic diagnostics $\frac{[NeV]14.3\mu m}{[NeII]12.8\mu m}$, $\frac{[NeV]24.3\mu m}{[NeII]12.8\mu m}$, $\frac{[OIV]25.9\mu m}{[NeII]12.8\mu m}$, $\frac{[NeIII]15.6\mu m}{[NeII]12.8\mu m}$, $\log\left(\frac{f_{30}}{f_{15}}\right)$, and $PAH\ 7.7\mu m$ and

linearly interpolating between AGN and starburst values we estimated that AGN contribute 17% of the sample's L_{FIR} .

5. Spectroscopy at wavelengths in the optical or near-infrared is likely to miss an AGN buried in extinction in these dusty infrared-bright galaxies.

8. Acknowledgments

This work is based [in part] on observations made with the Spitzer Space Telescope, which is operated by the Jet Propulsion Laboratory, California Institute of Technology under a contract with NASA. Support for this work was provided by NASA through an award issued by JPL/Caltech.

This research has made use of the NASA/IPAC Extragalactic Database (NED) which is operated by the Jet Propulsion Laboratory, California Institute of Technology, under contract with the National Aeronautics and Space Administration.

REFERENCES

- Armus, L., et al. 2007, *ApJ*, 656, 148
- Barnes, J. E., & Hernquist, L. 1992, *ARA&A*, 30, 705
- Barnes, J. E., & Hernquist, L. E. 1991, *ApJ*, 370, L65
- Brandl, B. R., et al. 2006, *ApJ*, 653, 1129
- Cid Fernandes, R., Heckman, T., Schmitt, H., González Delgado, R. M., & Storchi-Bergmann, T. 2001, *ApJ*, 558, 81
- Draine, B. T. 1989, in *ESA Special Publication, Vol. 290, Infrared Spectroscopy in Astronomy*, ed. B. H. Kaldeich, 93–98
- Farrah, D., et al. 2007, *ApJ*, 667, 149
- Genzel, R., et al. 1998, *ApJ*, 498, 579
- Goldader, J. D., Joseph, R. D., Doyon, R., & Sanders, D. B. 1997, *ApJS*, 108, 449
- Heckman, T. M., van Breugel, W., Miley, G. K., & Butcher, H. R. 1983, *AJ*, 88, 1077
- Ho, L. C., & Keto, E. 2007, *ApJ*, 658, 314
- Hopkins, P. F., Younger, J. D., Hayward, C. C., Narayanan, D., & Hernquist, L. 2010, *MNRAS*, 402, 1693
- Houck, J. R., et al. 2004, *ApJS*, 154, 18
- Joseph, R. D. 1999, *Ap&SS*, 266, 321
- Joseph, R. D., Meikle, W. P. S., Robertson, N. A., & Wright, G. S. 1984, *MNRAS*, 209, 111
- Joseph, R. D., & Wright, G. S. 1985, *MNRAS*, 214, 87

- Kartaltepe, J. S., et al. 2010, *ApJ*, 709, 572
- Larson, R. B., & Tinsley, B. M. 1978, *ApJ*, 219, 46
- Laurent, O., Mirabel, I. F., Charmandaris, V., Gallais, P., Madden, S. C., Sauvage, M., Vigroux, L., & Cesarsky, C. 2000, *A&A*, 359, 887
- Lutz, D., Spoon, H. W. W., Rigopoulou, D., Moorwood, A. F. M., & Genzel, R. 1998, *ApJ*, 505, L103
- Mihos, J. C., & Hernquist, L. 1996, *ApJ*, 464, 641
- Noguchi, M. 1988, *A&A*, 203, 259
- Peeters, E., Spoon, H. W. W., & Tielens, A. G. G. M. 2004, *ApJ*, 613, 986
- Petric, A. O., et al. 2011, *ApJ*, 730, 28
- Rieke, G. H., & Low, F. J. 1972, *ApJ*, 176, L95+
- Roche, P. F., Aitken, D. K., & Smith, C. H. 1991, *MNRAS*, 252, 282
- Rodriguez Espinosa, J. M., Rudy, R. J., & Jones, B. 1987, *ApJ*, 312, 555
- Sanders, D. B. 1999, *Ap&SS*, 266, 331
- Sani, E., Lutz, D., Risaliti, G., Netzer, H., Gallo, L. C., Trakhtenbrot, B., Sturm, E., & Boller, T. 2010, *MNRAS*, 403, 1246
- Schweizer, F. 2005, in *Astrophysics and Space Science Library*, Vol. 329, *Starbursts: From 30 Doradus to Lyman Break Galaxies*, ed. R. de Grijs & R. M. González Delgado, 143–+
- Shier, L. M., Rieke, M. J., & Rieke, G. H. 1996, *ApJ*, 470, 222

- Soifer, B. T., Sanders, D. B., Madore, B. F., Neugebauer, G., Danielson, G. E., Elias, J. H., Lonsdale, C. J., & Rice, W. L. 1987, *ApJ*, 320, 238
- Spinoglio, L., & Malkan, M. A. 1992, *ApJ*, 399, 504
- Storchi-Bergmann, T., González Delgado, R. M., Schmitt, H. R., Cid Fernandes, R., & Heckman, T. 2001, *ApJ*, 559, 147
- Sturm, E., Lutz, D., Verma, A., Netzer, H., Sternberg, A., Moorwood, A. F. M., Oliva, E., & Genzel, R. 2002, *A&A*, 393, 821
- Tielens, A. G. G. M., Peeters, E., Bakes, E. L. O., Spoon, H. W. W., & Hony, S. 2004, in *Astronomical Society of the Pacific Conference Series*, Vol. 323, *Star Formation in the Interstellar Medium: In Honor of David Hollenbach*, ed. D. Johnstone, F. C. Adams, D. N. C. Lin, D. A. Neufeld, & E. C. Ostriker, 135–+
- Toomre, A., & Toomre, J. 1972, *ApJ*, 178, 623
- Veilleux, S., et al. 2009, *ApJS*, 182, 628
- Verma, A., Lutz, D., Sturm, E., Sternberg, A., Genzel, R., & Vacca, W. 2003, *A&A*, 403, 829
- Weedman, D. W., et al. 2005, *ApJ*, 633, 706
- Werner, M. W., et al. 2004, *ApJS*, 154, 1
- Wright, G. S., Joseph, R. D., Robertson, N. A., James, P. A., & Meikle, W. P. S. 1988, *MNRAS*, 233, 1

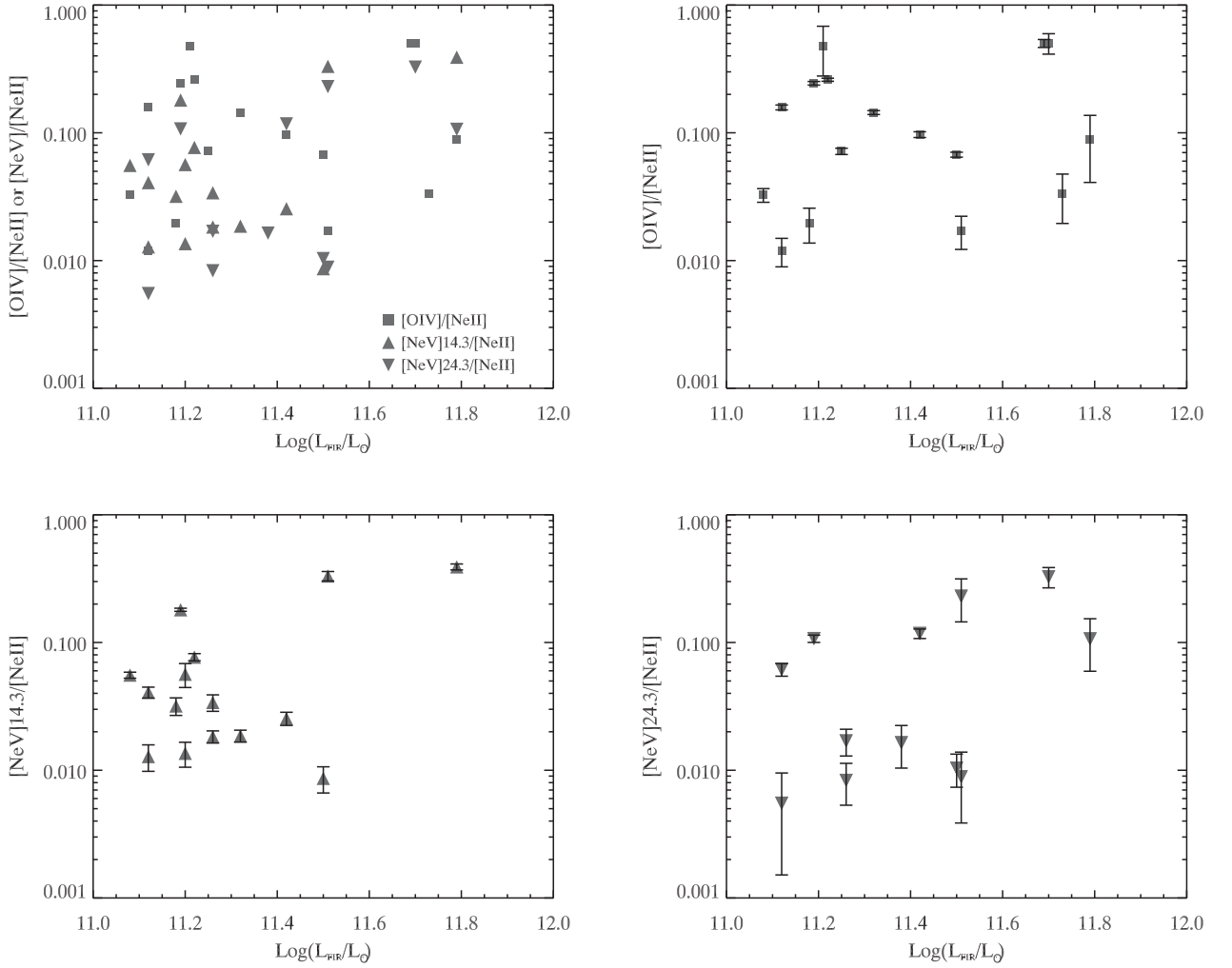


Fig. 1.— The $[OIV]25.9\mu m / [NeII]12.8\mu m$, $[NeV]14.3\mu m / [NeII]12.8\mu m$ and $[NeV]24.3\mu m / [NeII]12.8\mu m$ ratios from our sample of galaxies versus each galaxy’s FIR luminosity. The first panel shows a summary of all the data in the three following panels.

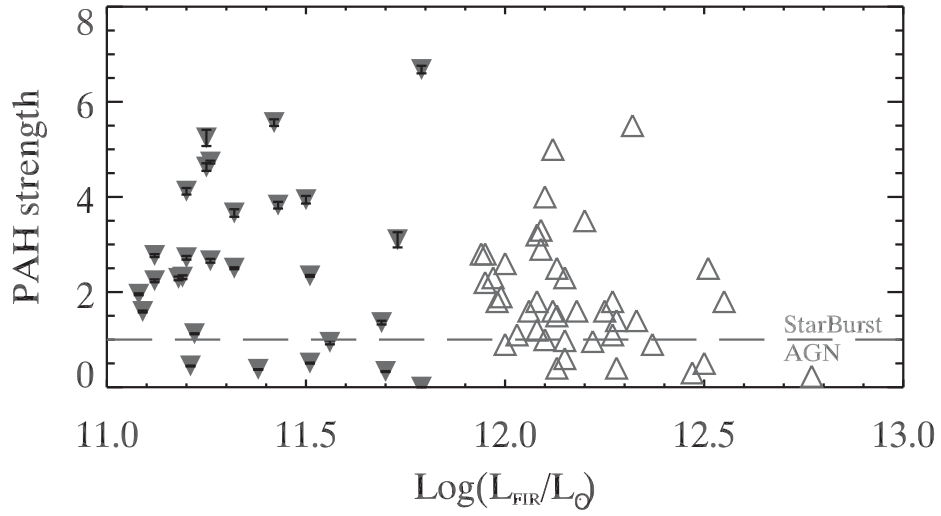


Fig. 2.— A comparison between the *PAH* $7.7\mu m$ strengths in our LIRG sample (the filled inverted triangles) and those of the ULIRG sample of Lutz et al. (1998) (the unfilled triangles), versus the FIR luminosity for each galaxy. The dashed line is the starburst/AGN discriminator suggested by Lutz et al. (1998).

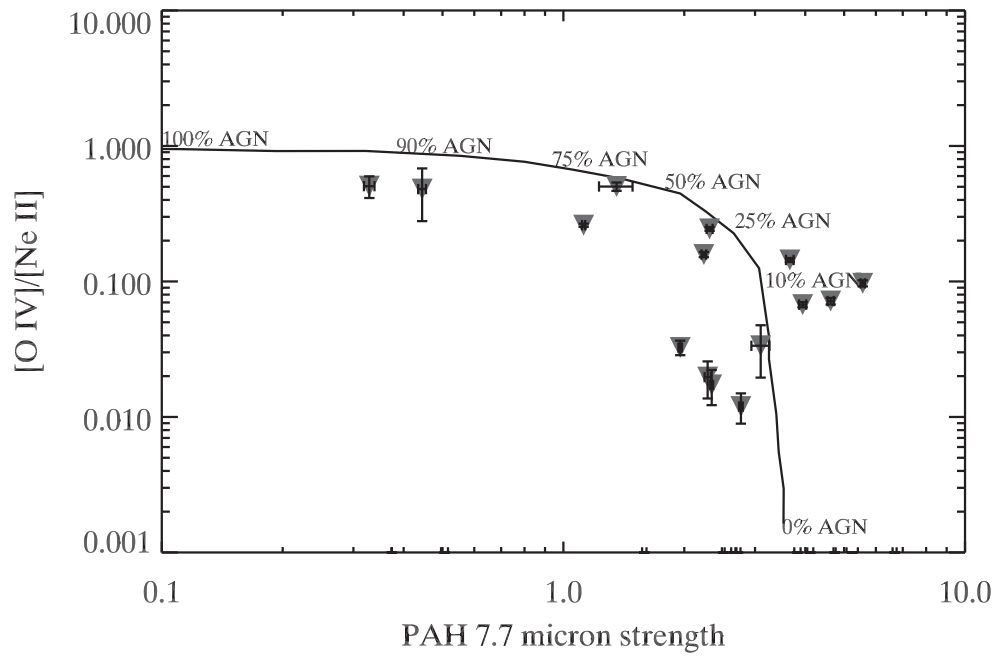


Fig. 3.— The $\frac{[O\ IV]_{25.9\mu m}}{[Ne\ II]_{12.8\mu m}}$ ratio versus the $PAH\ 7.7\mu m$ strength for each LIRG. Also shown is the Genzel et al. (1998) diagnostic curve with their percentage estimates of the AGN contribution along the curve.

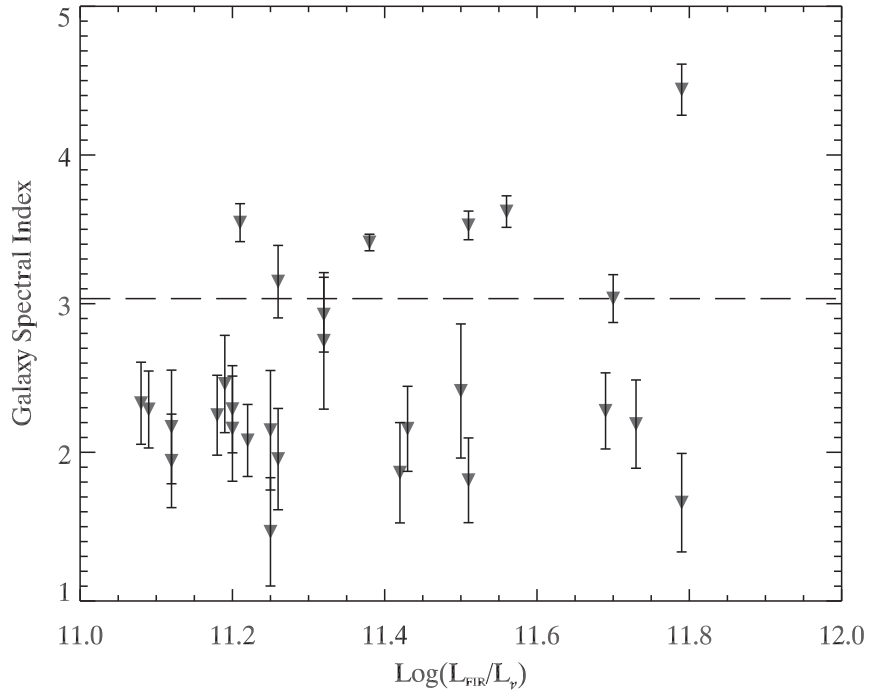


Fig. 4.— The spectral indices of the best fit slope to the 7-14 μ m wavelength range for each galaxy in our sample. The uncertainties are 1 sigma errors in the best fit spectral indices. The dashed line shows the spectral index above which galaxies have the power-law like spectra of AGN and below which galaxies have starburst like spectra.

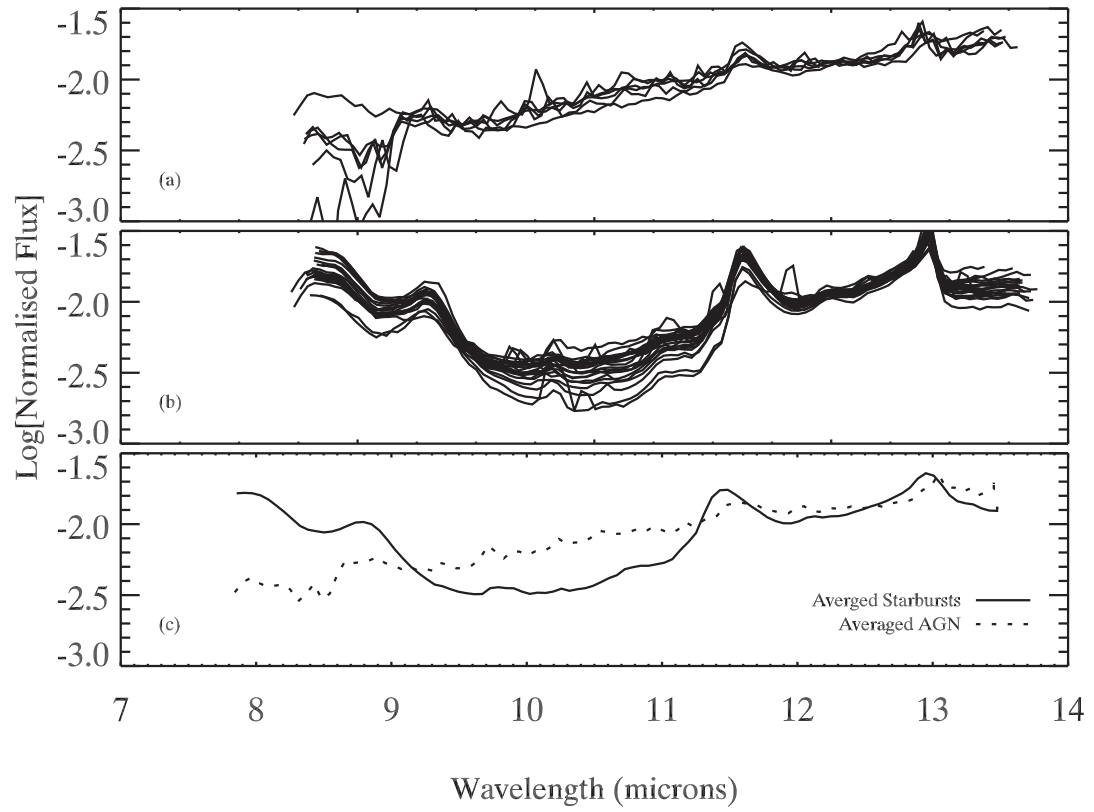


Fig. 5.— Panel (a) shows the normalized 7-14 μ m spectra of the galaxies that are well fit by an AGN-like power-law. Panel (b) shows the normalized spectra of galaxies that have starburst-like spectra. Panel (c) shows a comparison of the average normalized spectra from panels (a) and (b).

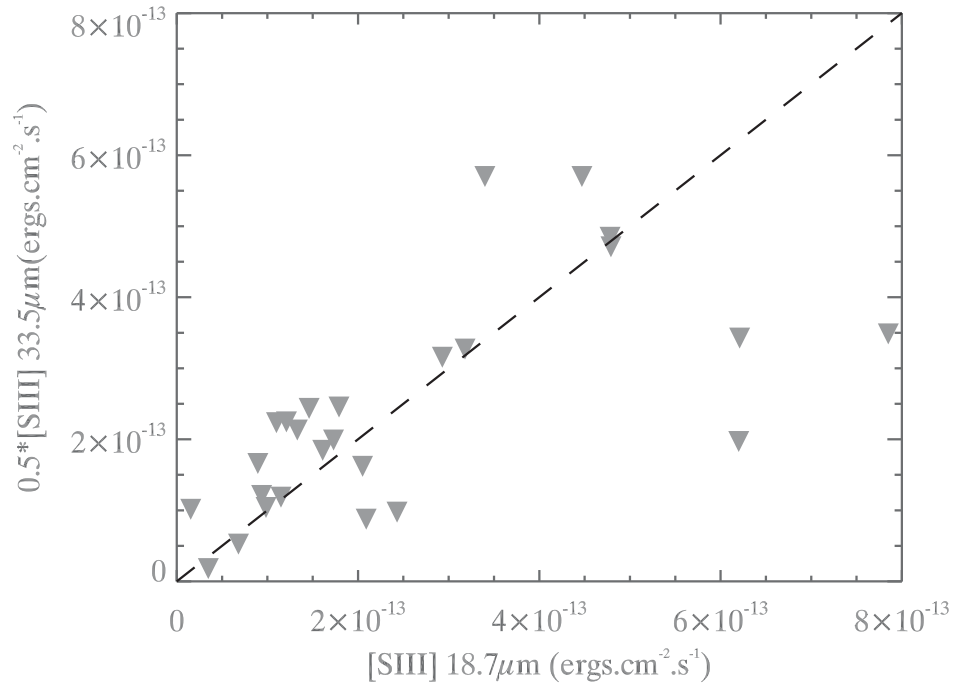


Fig. 6.— 0.5 times the flux of [SIII]33.5 μm versus the flux of [SIII]18.7 μm. The dashed line is the line of zero relative extinction and galaxies suffering from extinction will fall below this line.

Table 1: Observed LIRG Sample Properties

| ID ^a | Name | RA ^b | DEC | cz ^c Distance | | FIR luminosity Log(L _{FIR} /L _{sun}) |
|-----------------|---------------|--|-------------|--------------------------|-------|--|
| | | | | km/s | Mpc | |
| 1 | MCG-03-04-014 | 1 ^h 5 ^m 42 ^s | -17°7'1" | 10040 | 131.0 | 11.58 |
| 2 | IR01364-1042 | 1 ^h 36 ^m 24 ^s | -10°42'25" | 14250 | 187.2 | 11.76 |
| 3 | NGC695 | 1 ^h 48 ^m 28.1 ^s | 22°20'10" | 9769 | 129.8 | 11.64 |
| 4 | IR03359+1523 | 3 ^h 35 ^m 57.1 ^s | 15°23'6" | 10600 | 140.1 | 11.47 |
| 5 | UGC3094 | 4 ^h 32 ^m 38.3 ^s | 19°4'7" | 7407 | 98.1 | 11.36 |
| 6 | NGC2342 | 7 ^h 6 ^m 20.5 ^s | 20°43'4" | 5256 | 71.0 | 11.22 |
| 7 | NGC2388 | 7 ^h 25 ^m 38.2 ^s | 33°55'20" | 4060 | 56.4 | 11.18 |
| 8 | MCG+08-18-012 | 9 ^h 33 ^m 18.5 ^s | 48°41'53" | 7790 | 107.7 | 11.31 |
| 9 | NGC3110 | 10 ^h 1 ^m 32.2 ^s | -6°14'2" | 4840 | 66.0 | 11.22 |
| 10 | IR10173-0828 | 10 ^h 17 ^m 22.1 ^s | 8°28'41" | 14390 | 193.7 | 11.77 |
| 11 | MCG-00-29-023 | 11 ^h 18 ^m 38.6 ^s | -2°42'36" | 7230 | 98.6 | 11.23 |
| 12 | UGC6436 | 11 ^h 23 ^m 9.8 ^s | 14°56'53" | 10216 | 139.4 | 11.52 |
| 13 | Arp193 | 13 ^h 18 ^m 19 ^s | 34°23'49" | 6870 | 96.8 | 11.58 |
| 14 | MRK1490 | 14 ^h 17 ^m 53.76 ^s | 49°27'55.7" | 7696 | 108.0 | 11.32 |
| 15 | Arp302 | 14 ^h 54 ^m 47.8 ^s | 24°48'58" | 10100 | 139.7 | 11.65 |
| 16 | IZw107N | 15 ^h 16 ^m 19 ^s | 42°55'41" | 12043 | 166.0 | 11.85 |
| 17 | NGC6090 | 16 ^h 10 ^m 24 ^s | 52°35'6" | 8733 | 122.0 | 11.49 |
| 18 | IR16164-0746 | 16 ^h 16 ^m 29.5 ^s | -7°46'49" | 6857 | 94.8 | 11.43 |
| 19 | NGC6285 | 16 ^h 57 ^m 44.9 ^s | 59°0'40" | 5600 | 80.4 | 11.33 |
| 20 | NGC6286 | 16 ^h 57 ^m 44.9 ^s | 59°0'40" | 5600 | 80.4 | 11.33 |
| 21 | IR17132-5313 | 17 ^h 13 ^m 14.2 ^s | 53°13'52" | 15212 | 208.0 | 11.88 |
| 22 | IR17138-1017 | 17 ^h 13 ^m 50.7 ^s | -10°17'29" | 5261 | 73.1 | 11.39 |
| 23 | Zw448.020 | 20 ^h 55 ^m 5.3 ^s | 16°56'3" | 10900 | 147.4 | 11.89 |
| 24 | ESO602-G025 | 22 ^h 28 ^m 42.7 ^s | -19°17'31" | 7263 | 95.5 | 11.25 |
| 25 | UGC12150 | 22 ^h 38 ^m 53.6 ^s | 33°59'12" | 6413 | 87.6 | 11.29 |
| 26 | Zw453.062 | 23 ^h 2 ^m 28.1 ^s | 19°16'55" | 7373 | 99.1 | 11.28 |
| 27 | MCG+07-23-019 | 11 ^h 1 ^m 5.04 ^s | 41°7'7.6" | 10810 | 145.0 | 11.61 |
| 28 | CGCG052-037 | 16 ^h 28 ^m 27.22 ^s | 4°11'23.2" | 7342 | 103.0 | 11.38 |

^a Col 1 is the galaxy ID.

^b RA and DEC in B1950.

^c Col 5,6,7 are from (Goldader et al. 1997).

Table 2: Coronal diagnostic line ratios and a rough estimate of percentage AGN contribution.

| Name | $\frac{[NeV]24.3\mu m}{[NeII]12.8\mu m}$ | Error | AGN (%) | $\frac{[NeV]14.3}{[NeII]12.8\mu m}$ | Error | AGN (%) | $\frac{[OIV]25.9\mu m}{[NeII]12.8\mu m}$ | Error | AGN (%) |
|---------------|--|-------|---------|-------------------------------------|-------|---------|--|-------|---------|
| MCG-03-04-014 | 0.117 | 0.010 | 39 | 0.025 | 0.003 | 6 | 0.097 | 0.005 | 10 |
| IR01364-1042 | | | | | | | 0.502 | 0.036 | 50 |
| NGC695 | 0.009 | 0.005 | 3 | | | | 0.017 | 0.005 | 2 |
| IR03359+1523 | 0.016 | 0.006 | 5 | | | | | | |
| UGC3094 | | | | 0.077 | 0.005 | 19 | 0.260 | 0.007 | 26 |
| GC2342 | | | | 0.032 | 0.005 | 8 | 0.020 | 0.006 | 2 |
| NGC2388 | | | | 0.056 | 0.003 | 14 | 0.033 | 0.004 | 3 |
| MCG+08-18-012 | | | | | | | 0.480 | 0.202 | 48 |
| NGC3110 | 0.006 | 0.004 | 2 | 0.013 | 0.003 | 3 | 0.012 | 0.003 | 1 |
| IR10173-0828 | 0.326 | 0.059 | 109 | | | | 0.505 | 0.092 | 50 |
| MCG-00-29-023 | | | | | | | | | |
| UGC6436 | | | | | | | | | |
| Arp193 | 0.010 | 0.003 | 3 | 0.009 | 0.002 | 2 | 0.067 | 0.003 | 7 |
| MRK1490 | | | | 0.014 | 0.003 | 3 | | | |
| Arp302 | | | | | | | | | |
| IZw107N | | | | | | | 0.034 | 0.014 | 3 |
| NGC6090 | | | | | | | | | |
| IR16164-0746 | | | | 0.019 | 0.002 | | 0.144 | 0.005 | 15 |
| NGC6285 | | | | | | | | | |
| IR17132-5313 | | | | | | | 0.072 | 0.004 | 13 |
| IR17132-5313 | | | | | | | | | |
| IR17138-1017 | 0.017 | 0.004 | 6 | 0.034 | 0.005 | 8 | | | |
| Zw448.020 | 0.107 | 0.047 | 36 | 0.391 | 0.021 | 98 | 0.089 | 0.048 | 9 |
| ESO602-G025 | 0.062 | 0.007 | 20 | 0.041 | 0.004 | 10 | 0.158 | 0.007 | 16 |
| UGC12150 | | | | 0.057 | 0.012 | 14 | | | |
| Zw453.062 | 0.107 | 0.007 | 36 | 0.181 | 0.005 | 45 | 0.244 | 0.008 | 24 |
| MCG+07-23-019 | 0.230 | 0.085 | 77 | 0.332 | 0.028 | 83 | | | |
| cgcg052-037 | 0.008 | 0.003 | 3 | 0.018 | 0.002 | 5 | | | |

^a Rough percentage AGN contributions are estimated by linearly interpolating between the median AGN and starburst line ratios given in Sturm et al. (2002).

Table 3: The fluxes measured for each galaxy in units of $10^{-14}(\text{ergs}/\text{cm}^2/\text{s})$, also shows the star formation rate based on the luminosity of ($[\text{Ne II}] + [\text{Ne III}]$) and lists the PAH strengths.

| Galaxy | [Ne V] 14.3 μm | | [Ne V] 24.3 μm | | [O IV] 25.9 μm | | [Ne II] 12.8 μm | | [Ne III] 15.55 μm | | [S III] 18.7 μm | | [S III] 33.48 μm | | Star ^a Formation Rate (M sun/yr) | | PAH ^b Strength 7.7 μm | | Error AGN ^c (%) | | Jansky ^e f_{30} | | f_{15} Jansky | | $L_{\text{og}}(\frac{\text{Jn}}{\%})$ | | Error AGN ^d (%) | | |
|---------------|---------------------------|-------|---------------------------|-------|---------------------------|-------|----------------------------|-------|------------------------------|-------|----------------------------|-------|-----------------------------|-------|--|-------|---|-------|----------------------------|-------|------------------------------|-------|-----------------|-------|---------------------------------------|-------|----------------------------|-------|-----|
| | Flux | Error | Flux | Error | Flux | Error | Flux | Error | Flux | Error | Flux | Error | Flux | Error | Rate | Error | Rate | Error | Strength | Error | AGN | Error | Jansky | Error | Jansky | Error | Log | Error | AGN |
| MCG-03-04-014 | 2.36 | 0.29 | 10.86 | 0.94 | 8.99 | 0.49 | 92.85 | 0.46 | 13.06 | 0.36 | 47.85 | 1.3 | 96.89 | 1.02 | 135 | 3.4 | 5.56 | 0.07 | 0 | 0 | 2.37 | 0.28 | 0.93 | 0.012 | 46 | 0.93 | 0.012 | 46 | |
| IR01364+1042 | | | 8.08 | 0.43 | 16.13 | 0.78 | 3.35 | 0.28 | 1.54 | 0.3 | 20.31 | 0.84 | 47 | 4.6 | 1.36 | 0.04 | 74 | 1.68 | 0.13 | 1.11 | 0.007 | 32 | 1.68 | 0.13 | 1.11 | 0.007 | 32 | | |
| NGC695 | | | 0.66 | 0.37 | 1.29 | 0.35 | 74.88 | 0.4 | 12.53 | 0.31 | 29.32 | 0.88 | 63.11 | 1.24 | 102 | 2.6 | 2.34 | 0.02 | 4 | 1.57 | 0.25 | 0.8 | 0.015 | 56 | 0.8 | 0.015 | 56 | | |
| IR03359+1523 | | | 0.85 | 0.3 | | | 52.01 | 0.83 | 16.04 | 0.24 | 24.31 | 0.3 | 19.55 | 0.92 | 84 | 2 | 0.37 | 0 | 100 | 1.36 | 0.3 | 0.66 | 0.029 | 66 | 0.66 | 0.029 | 66 | | |
| UGC3094 | 3.75 | 0.23 | | | 12.68 | 0.32 | 48.82 | 0.48 | 18.84 | 0.26 | 78.52 | 2.75 | 69.7 | 0.88 | 45 | 0.8 | 1.12 | 0.01 | 91 | 1.68 | 0.26 | 0.81 | 0.02 | 55 | 0.81 | 0.02 | 55 | | |
| NGC2342 | 1.49 | 0.25 | | | 0.92 | 0.27 | 46.8 | 0.32 | 7.42 | 0.24 | 16.1 | 2.52 | 36.94 | 0.99 | 19 | 0.6 | 2.29 | 0.04 | 8 | 1.36 | 0.14 | 0.99 | 0.008 | 42 | 0.99 | 0.008 | 42 | | |
| NGC2388 | 6.72 | 0.41 | | | 3.94 | 0.54 | 120.93 | 0.5 | 12.94 | 0.36 | 61.98 | 3.51 | 39.44 | 1.54 | 30 | 0.8 | 1.95 | 0.02 | 32 | 5.31 | 0.41 | 1.11 | 0.006 | 32 | 1.11 | 0.006 | 32 | | |
| MCG+08-18-012 | | | 0.44 | 0.18 | | | 0.92 | 0.12 | | | | | 3.61 | 0.58 | 1 | 0 | 0.44 | 0.01 | 100 | 0.12 | 0.03 | 0.6 | 0.024 | 70 | 0.6 | 0.024 | 70 | | |
| NGC3110 | 1.17 | 0.26 | 0.5 | 0.32 | 1.09 | 0.32 | 91.39 | 0.39 | 10.94 | 0.23 | 62.1 | 2.85 | 68.48 | 1.08 | 31 | 0.7 | 2.77 | 0.03 | 0 | 1.69 | 0.18 | 0.97 | 0.006 | 43 | 0.97 | 0.006 | 43 | | |
| IR10173-0828 | | | 0.98 | 0.17 | 1.51 | 0.27 | 2.99 | 0.11 | | | | | 4.16 | 0.57 | 8 | 0 | 0.33 | 0.01 | 100 | 1.69 | 0.21 | 0.91 | 0.01 | 48 | 0.91 | 0.01 | 48 | | |
| MCG-06-29-023 | | | | | 40.4 | 0.57 | | | 8.03 | 0.34 | 13.31 | 0.67 | 42.59 | 0.83 | 33 | 1.4 | 1.59 | 0.02 | 58 | 2.12 | 0.34 | 0.79 | 0.015 | 56 | 0.79 | 0.015 | 56 | | |
| UGC6436 | | | | | 29.8 | 0.23 | | | 3.13 | 0.22 | 9.85 | 0.52 | 20.78 | 0.72 | 44 | 3.1 | 3.83 | 0.07 | 0 | 1.31 | 0.16 | 0.91 | 0.014 | 47 | 0.91 | 0.014 | 47 | | |
| Arp103 | 1.2 | 0.22 | 1.44 | 0.45 | 9.38 | 0.47 | 138.81 | 0.42 | 25.9 | 0.26 | 34.05 | 0.47 | 113.53 | 1.95 | 107 | 1.1 | 3.94 | 0.08 | 0 | 4.71 | 0.22 | 1.33 | 0.002 | 16 | 1.33 | 0.002 | 16 | | |
| MRK1490 | 0.72 | 0.18 | | | 52.83 | 0.41 | | | 5.18 | 0.21 | 20.94 | 1.68 | 17.49 | 1.23 | 47 | 1.9 | 4.12 | 0.07 | 0 | 2.12 | 0.2 | 1.03 | 0.005 | 39 | 1.03 | 0.005 | 39 | | |
| Arp302 | | | | | 0.67 | 0.28 | 19.9 | 0.74 | 4.81 | 0.38 | 6.81 | 0.36 | 10.49 | 0.83 | 47 | 4.1 | 3.1 | 0.16 | 0 | 0.75 | 0.08 | 0.97 | 0.01 | 43 | 0.97 | 0.01 | 43 | | |
| IzW107N | | | | | 95.92 | 0.56 | | | 26.15 | 0.31 | 47.86 | 7.76 | 94.23 | 0.92 | 126 | 1.7 | 2.5 | 0.02 | 0 | 2.2 | 0.24 | 0.96 | 0.008 | 44 | 0.96 | 0.008 | 44 | | |
| NGC6090 | | | | | 10.03 | 0.31 | 69.36 | 0.34 | 24.32 | 0.2 | 10.96 | 0.31 | 44.73 | 1.01 | 58 | 0.6 | 3.66 | 0.08 | 0 | 2.85 | 0.15 | 1.28 | 0.004 | 20 | 1.28 | 0.004 | 20 | | |
| IR16164+0746 | 1.29 | 0.17 | | | 28.16 | 0.32 | | | 4.31 | 0.19 | 20.48 | 1.91 | 32.37 | 6.4 | 15 | 0.7 | 5.24 | 0.17 | 0 | 0.49 | 0.04 | 1.09 | 0.01 | 34 | 1.09 | 0.01 | 34 | | |
| NGC6285 | | | 3.59 | 0.18 | | | 50.06 | 1.12 | 6.77 | 0.21 | 12.09 | 1.63 | 44.86 | 7.98 | 26 | 1 | 4.63 | 0.08 | 0 | 1 | 0.09 | 1.05 | 0.012 | 37 | 1.05 | 0.012 | 37 | | |
| IR17132-5313 | | | | | 50.26 | 0.13 | | | 5.63 | 0.19 | 17.9 | 0.32 | 49.11 | 1.05 | 168 | 5.7 | 6.68 | 0.08 | 0 | 1.65 | 0.16 | 1.01 | 0.007 | 40 | 1.01 | 0.007 | 40 | | |
| IR17132-5313 | | | | | 130.05 | 0.68 | | | 24.42 | 0.47 | 44.68 | 3.42 | 114.07 | 1.63 | 57 | 1.1 | 4.73 | 0.03 | 0 | 3.75 | 0.31 | 1.08 | 0.007 | 35 | 1.08 | 0.007 | 35 | | |
| IR17138-1017 | 4.41 | 0.6 | 2.2 | 0.48 | | | 29.08 | 0.26 | 13.97 | 0.15 | 11.48 | 1.19 | 23.74 | 0.85 | 29 | 0.4 | 2.31 | 0.04 | 6 | 1.83 | 0.14 | 1.12 | 0.007 | 32 | 1.12 | 0.007 | 32 | | |
| Zw448-020 | 2.7 | 0.12 | 0.74 | 0.33 | 0.61 | 0.33 | 6.91 | 0.22 | 4.02 | 0.15 | 9.36 | 0.55 | 24.22 | 0.98 | 16 | 0.8 | 0.01 | 0 | 100 | 0.91 | 0.12 | 0.88 | 0.002 | 50 | 0.88 | 0.002 | 50 | | |
| ESO002-G025 | 2.26 | 0.23 | 3.41 | 0.37 | 8.77 | 0.38 | 55.52 | 0.39 | 13.04 | 0.21 | 17.27 | 2.02 | 39.79 | 1.25 | 43 | 0.8 | 2.24 | 0.03 | 11 | 2.11 | 0.27 | 0.89 | 0.014 | 49 | 0.89 | 0.014 | 49 | | |
| UGC12150 | 1.41 | 0.29 | | | 25.02 | 0.43 | | | 6.79 | 0.28 | 14.57 | 2.62 | 48.66 | 1.5 | 17 | 0.8 | 2.72 | 0.04 | 0 | 2.5 | 0.17 | 1.17 | 0.003 | 28 | 1.17 | 0.003 | 28 | | |
| Zw453-062 | 5.25 | 0.14 | 3.12 | 0.21 | 7.11 | 0.21 | 29.08 | 0.26 | 13.97 | 0.15 | 11.48 | 1.19 | 23.74 | 0.85 | 29 | 0.4 | 2.31 | 0.04 | 6 | 1.83 | 0.14 | 1.12 | 0.007 | 32 | 1.12 | 0.007 | 32 | | |
| MCG+07-23-019 | 0.9 | 0.07 | 0.62 | 0.23 | | | 2.71 | 0.08 | 2.12 | 0.09 | 8.95 | 0.5 | 33.25 | 1.09 | 7 | 0.4 | 0.51 | 0.01 | 100 | 1.29 | 0.11 | 1.07 | 0.006 | 36 | 1.07 | 0.006 | 36 | | |
| CGCG052-037 | 1.67 | 0.18 | 0.76 | 0.32 | | | 91.21 | 0.41 | 8.43 | 0.2 | 31.78 | 0.44 | 65.36 | 0.91 | 73 | 1.8 | 2.66 | 0.04 | 0 | 2.24 | 0.23 | 0.99 | 0.006 | 42 | 0.99 | 0.006 | 42 | | |

^aDetermined from the ($L_{[\text{Ne II}]12.8\mu\text{m}} + L_{[\text{Ne III}]15.6\mu\text{m}}$) and the calibration of Ho & Keto (2007).

^bPAH 7.7 μm strength as defined by Lutz et al. (1998).

^cEstimate of the percentage AGN contribution to luminosity using PAH 7.7 μm with linear interpolating between starburst = 2.4 and AGN = 1

^dEstimate of the percentage AGN contribution to luminosity using $\log(\frac{f_{30}}{f_{15}})$ with linear interpolating between starburst = 1.55 and AGN = 0.2.

Table 4: $[NeIII]15.6\mu m / [NeII]12.8\mu m$ and extinction estimates.

| Name | $\frac{[NeIII]15.6\mu m^a}{[NeII]12.8\mu m}$ | Error | % AGN ^b | $\frac{[SIII]18.7\mu m}{[SIII]33.5\mu m}$ | Error | Extinction ^c | |
|---------------|--|-------|--------------------|---|-------|-------------------------|------------------------------|
| | | | | | | Relative (Mags) | A_v ^d (Mags) |
| MCG-03-04-014 | 0.13 | 0.004 | 3 | 0.49 | 0.014 | 0.01 | 0.46 |
| IR01364-1042 | 0.18 | 0.02 | 9 | 0.08 | 0.015 | | |
| NGC695 | 0.15 | 0.004 | 6 | 0.46 | 0.017 | 0.08 | 2.71 |
| IR03359+1523 | 0.27 | 0.007 | 19 | 1.24 | 0.061 | | |
| UGC3094 | 0.34 | 0.007 | 27 | 1.13 | 0.042 | | |
| NGC2342 | 0.14 | 0.005 | 4 | 0.44 | 0.069 | 0.15 | 5.07 |
| NGC2388 | 0.09 | 0.003 | 0 | 1.57 | 0.108 | | |
| MCG+08-18-012 | | | | | | | |
| NGC3110 | 0.11 | 0.003 | 1 | 0.91 | 0.044 | | |
| IR10173-0828 | | | | | | | |
| MCG-00-29-023 | 0.17 | 0.009 | 8 | 0.31 | 0.017 | 0.51 | 17.36 |
| UGC6436 | 0.09 | 0.007 | 0 | 0.47 | 0.03 | 0.06 | 1.98 |
| Arp193 | 0.16 | 0.002 | 7 | 0.3 | 0.007 | 0.56 | 18.87 |
| MRK1490 | 0.09 | 0.004 | 0 | 1.2 | 0.128 | | |
| Arp302 | | | | 0.97 | 0.224 | | |
| IZw107N | 0.21 | 0.021 | 12 | 0.65 | 0.062 | | |
| NGC6090 | 0.24 | 0.004 | 16 | 0.51 | 0.083 | | |
| IR16164-0746 | | 0.003 | | 0.25 | 0.009 | 0.77 | 26.33 |
| NGC6285 | 0.05 | 0.007 | 0 | 0.63 | 0.138 | | |
| IR17132-5313 | 0.21 | 0.005 | 12 | 0.27 | 0.06 | 0.67 | 22.83 |
| IR17132-5313 | 0.1 | 0.004 | 0 | 0.36 | 0.01 | 0.34 | 11.67 |
| IR17138-1017 | 0.16 | 0.004 | 7 | 0.39 | 0.031 | 0.27 | 9.02 |
| Zw448.020 | 1.66 | 0.028 | 100 | 0.39 | 0.028 | 0.28 | 9.51 |
| ESO602-G025 | 0.11 | 0.004 | 1 | 0.43 | 0.053 | 0.15 | 5.22 |
| UGC12150 | 0.49 | 0.012 | 43 | 0.3 | 0.055 | 0.56 | 18.92 |
| Zw453.062 | 0.06 | 0.007 | 0 | 0.48 | 0.053 | 0.04 | 1.25 |
| MCG+07-23-019 | 2.73 | 0.04 | 100 | 0.27 | 0.017 | 0.67 | 22.87 |
| cgcg052-037 | | 0.002 | | 0.49 | 0.01 | 0.03 | 1.03 |

^a [Ne III] to [Ne II] flux ratio.

^b The estimated percentage AGN contribution to L_{FIR} based on linearly interpolating between 1.0 (100% AGN) and 0.1 (0% AGN).

^c Lower limit to relative extinction estimated using the [S III]18.7 μm to [S III] 33.5 μm ratio.

^d Lower limit to V-band extinction based on Draine (1989).

Table 5: The Spectral Indices for galaxies that have AGN power-law shapes.

| Name | α | $\delta\alpha^a$ |
|---------------|----------|------------------|
| IR03359+1523 | 3.41 | ± 0.06 |
| MCG+08-18-012 | 3.54 | ± 0.13 |
| IR10173-0828 | 3.03 | ± 0.16 |
| Arp302 | 3.62 | ± 0.11 |
| Zw448.020 | 4.44 | ± 0.17 |
| MCG+07-23-019 | 3.53 | ± 0.10 |

^a 1 sigma errors in the spectral index.

Table 6: NASA Extragalactic Database classification.

| Name | NED Luminosity Class/Morphology ^a | Band Pass |
|-----------------|--|-------------|
| mcg-03-04-014 | LIRG , HII | Optical; IR |
| IRAS 01364-1042 | LINER;LIRG, HII | Optical; IR |
| NGC 695 | S0 pec;LIRG HII | Optical; IR |
| IRAS 03359+1523 | | Optical; IR |
| ugc3094 | LIRG; Sbc | Optical; IR |
| NGC 2342 | S pec HII; LIRG | Optical; IR |
| NGC 2388 | S; HII | Optical; IR |
| MCG +07-23-019 | | |
| NGC 3110 | SB(rs)b pec;HII;LIRG | Optical; IR |
| IRAS 10173-0828 | | |
| MCG +08-18-012 | HII | Optical |
| UGC 06436 | SB;LINER;LIRG HII | Optical; IR |
| ARP193 | Im: pec;HII LINER | Optical; IR |
| MRK 1490 | Sa;LINER;LIRG HII | Optical; IR |
| ARP302 | | Optical |
| IZw107N | | |
| NGC 6090 | S0/Sa pair; LIRG | Optical; IR |
| IRAS 16164-0746 | LINER; LIRG | Optical; IR |
| NGC 6285 | S0;LINER HII | Optical |
| NGC 6286 | Sb: pec; HII LINER; LIRG | Optical; IR |
| IRAS 17132-5313 | | |
| IRAS 17138-1017 | S; HII | Optical; IR |
| ZW448.020 | HI; LIRG; Pair | Optical; IR |
| ESO 602-G025 | SA(r)b;LIRG;HII; LINER | Optical; IR |
| UGC 12150 | SB0/a;HII;LINER | Optical; IR |
| ZW 453.062 | LIRG ; LINER | Optical; IR |
| MCG +00-29-023 | SAB(s)b;HII Sy2 | Optical; IR |
| CGCG 052-037 | S;LINER;LIRG HII | Optical; IR |

^a Uses the same notation as found in NED to describe classification.

Table 7: Results summary.

| Name | $\frac{[NeV]14.3\mu m}{[NeII]12.8\mu m}$ ^a | $\frac{[NeV]24.3\mu m}{[NeII]12.8\mu m}$ | $\frac{[OIV]25.9\mu m}{[NeII]12.8\mu m}$ | $\frac{[NeIII]15.6\mu m}{[NeII]12.8\mu m}$ ^b | PAH 7.7 μm Strength ^c | $\log\left(\frac{f_{30\mu m}}{f_{15\mu m}}\right)$ ^d | Power-law Continuum ^e |
|---------------|---|--|--|---|---------------------------------------|---|----------------------------------|
| MCG-03-04-014 | | SB-AGN | SB-AGN | | | | |
| IR01364-1042 | | | AGN | | AGN | | |
| NGC695 | | | | | SB-AGN | AGN | |
| IR03359+1523 | | | | | AGN | AGN | AGN |
| UGC3094 | | | AGN | | AGN | AGN | |
| NGC2342 | | | | | SB-AGN | | |
| NGC2388 | | | | | | | |
| MCG+08-18-012 | | | AGN | | AGN | AGN | AGN |
| NGC3110 | | | | | | | |
| IR10173-0828 | | AGN | AGN | | AGN | | AGN |
| MCG-00-29-023 | | | | | AGN | | |
| UGC6436 | | | | | | | |
| Arp193 | | | | | | | |
| MRK1490 | | | | | | | |
| Arp302 | | | | | AGN | AGN | AGN |
| IZw107N | | | | | | | |
| NGC6090 | | | | | SB-AGN | | |
| IR16164-0746 | | | | | | | |
| NGC6285 | | | | | | | |
| IR17132-5313 | | | SB-AGN | | | | |
| IR17132-5313 | | | | | | | |
| IR17138-1017 | | | | | | | |
| Zw448.020 | AGN | SB-AGN | | AGN | AGN | AGN | AGN |
| ESO602-G025 | | | | | SB-AGN | | |
| UGC12150 | | | | | | | |
| Zw453.062 | SB-AGN | SB-AGN | AGN | | | | |
| MCG+07-23-019 | AGN | | | AGN | AGN | | AGN |
| cgcg052-037 | | | | | | | |

^a Line ratios $[NeV]14.3\mu m/[NeII]12.8\mu m$, $[NeV]24.3\mu m/[NeII]12.8\mu m$ and $[OIV]25.9\mu m/[NeII]12.8\mu m$ above 50% of level for the AGN of Sturm et al. (2002) \implies AGN (significant AGN contribution) and line ratios above 25% of level for the AGN of Sturm et al. (2002) \implies SB-AGN (some AGN contribution but AGN is not dominant).

^b The AGN in Sturm et al. (2002), have a median $[NeIII]15.6\mu m/[NeII]12.8\mu m$ of 1.1, and their starburst templates have a median value of 0.1. A value above 1.1 for this line ratio \implies AGN (significant AGN contribution), and a line ratio of 0.35 (linearly interpolated to 25% of the AGN ratio) \implies SB-AGN (some AGN contribution but AGN is not dominant).

^c Genzel et al. (1998) template starbursts have average PAH strengths of 3.1 and their AGN templates have average PAH strengths of 2.1, with a standard deviation of about 1.0 in each case. We assume a PAH strength of 1.0 is \sim 100% AGN-dominated and linearly interpolate between 3.1 and 1.0 to estimate an approximate percentage contribution. Galaxies with PAH derived AGN contributions above 50% \implies AGN (significant AGN contribution). Galaxies with PAH derived AGN contributions above 25% \implies SB-AGN (some AGN contribution but AGN is not dominant).

^d The linear calibration of Veilleux et al. (2009) is assumed to drive approximate AGN contributions. Galaxies with $\log\left(\frac{f_{30}}{f_{15}}\right)$ AGN contributions above 50% of this linear calibration \implies AGN (significant AGN contribution).

^e Galaxies with continua that are well fit by power-law \implies AGN.